Nexus of Future Materials 1 (2024) 108-119

Nexus of Future Materials

https://nfmjournal.com/

# A Comprehensive Study of the Effect of BaO Doping on the Physical, Mechanical, Optical, and Radiation-Shielding Properties of Borate-Based Glasses

Shrikant Biradar, Ashok Dinkar, G.B. Devidas*

Department of Physics, Kuvempu University, Shankaraghatta, Shimoga-577 451, India

***Keywords:***

Barium-borate glasses
XRD
Physical properties
Optical parameters
Radiation shielding

**Abstract**

This study aimed to explore the physical, mechanical, optical, and radiation-attenuation characteristics of borate-based glasses with the composition (70-x)$B_2O_3$-28$Na_2O$-2$Gd_2O_3$-xBaO (where x = 0, 5, 10, 15, and 20 mol%). The glasses were fabricated via the melt-quenching approach, and their amorphous structures validated through X-ray diffraction analysis. The density of the glasses increased from 2.412 to 3.114 g/cm$^3$ due to the effective incorporation of barium oxide (BaO). The mechanical properties, assessed using the Makishima–Mackenzie model, showed a decrease in the mechanical moduli as the BaO content in the fabricated glasses increased. Optical analysis revealed a 3.048 to 2.807 eV decline in the indirect optical band gap energy and a 2.384 to 2.449 elevation in the refractive index as the BaO loading rose from 0 to 20 mol%, resulting in structural changes within the glass network and the generation of non-bridging oxygens. Additionally, radiation-shielding studies were carried out to determine the mass attenuation coefficient (MAC), half-value layer (HVL), and mean free path (MFP) using the XCOM software, revealing that the incorporation of BaO significantly enhanced the radiation-shielding performance of the prepared glasses, among which the glass with 20 mol% BaO (B-20) was the most effective for gamma-ray shielding through exhibiting high MAC and low HVL and MFP values. Furthermore, the evaluated MAC values were compared with those of recognized shielding materials and other BaO-doped glasses at 0.662 MeV, whereby the comparison verified that the glass with the highest BaO concentration provided the optimum radiation-shielding effectiveness, and is thus appropriate for radiation-protection applications.

## 1. Introduction

The growing use of radiation in various everyday applications such as medicine, scientific research, security, nuclear engineering, and industry has become a prominent feature of modern society [1, 2].

* Corresponding author:
E-mail address: devidasgb02@gmail.com
Received 29 August 2024; Accepted 23 September 2024; Published 25 September 2024,
https://doi.org/10.70128/584259

Since prolonged exposure to radiation sources poses a significant threat to both human health and the environment, it is crucial to explore innovative materials that can provide effective radiation protection, driven by the urgent need to mitigate the hazards associated with radiation exposure [3, 4].

Conventionally, concrete and lead compounds have represented the primary materials employed for radiation shielding. However, concrete's effectiveness diminishes at high temperatures, rendering it an inadequate solution.

Moreover, while lead and its compounds have shown better performance, they are limited by their toxicity, low melting point (327°C), poor chemical stability, and limited flexibility that restrict their widespread use [1, 4]. Hence, researchers have continued their search for an alternative radiation-shielding material that is characterized by transparency, with glass attracting their attention. Oxide glasses can be categorized into several types, including borates, silicate, tellurite, and phosphates. Among these, borate glasses have emerged as a versatile option due to their desirable characteristics that include lower melting temperatures, high transparency, superior thermal stability, outstanding mechanical durability, and corrosion resistance. Borate glasses doped with various divalent cations demonstrate improved properties, making them ideal for optical and attenuation applications [3, 5]. Particularly in the context of radiation-shielding materials, high transmission in the visible range is essential. In light of this, barium oxide (BaO) was carefully selected as the dopant for the present glass system, since it functions as a modifying oxide that optically enhances the glass by increasing the refractive index and imparting a vitreous luster while promoting transparency. In terms of radiation attenuation, the doping of BaO has shown significant advancements. With its high density (5.72 g/cm$^3$), substantial molar mass (153.33 g/mol), and effective attenuation coefficient, BaO greatly enhances the glass's ability to absorb radiation, thereby improving its shielding characteristics [4, 6, 7]. Sodium oxide ($Na_2O$) is employed to broaden the glass-forming range, reducing the melting temperature and facilitating ion exchange. This results in the creation of a glass with a lower melting point, which is being further investigated for its potential in gamma-ray protection [8]. With a density of 7.41 g/cm$^3$, gadolinium oxide ($Gd_2O_3$) is a good rare-earth ion that exhibits enhanced shielding properties when co-doped with other oxides in a glass composition. The addition of $Gd_2O_3$ to the glass increases its density, thereby boosting its shielding ability [5, 9].Increasing interest has focused on developing specialized glasses for gamma-ray protection. A detailed review of the literature on barium-borate glasses has provided important insights into distinguishing between different glass compositions. For instance, Biradar et al. [10] explored how BaO affects various properties of $B_2O_3$-$Bi_2O_3$-ZnO-$WO_3$ glass systems, whereby the glass containing higher BaO (20 mol%) content manifested the greatest shielding capability among those synthesized. Zakaly et al. [3] investigated how BaO influences the shielding characteristics of alumino-borate glass networks by comparing the experimental findings with theoretical predictions for shielding coefficients, including the linear attenuation coefficient (LAC), mass attenuation coefficient (MAC), half-value layer (HVL), and tenth-value layer. Sayyed et al. [4] explored the effects of BaO addition on the structure, linear/non-linear optical characteristics, and radiation-attenuation efficiency of $B_2O_3$-NiO-BaO-ZnO glasses, reporting that the glass composition with 32 mol% BaO exhibited superior shielding performance, characterized by high MAC and low MFP and HVL values. They also compared the HVL values of their glasses with those of previously studied BaO-containing glasses to better understand the radiation protection offered by their prepared glasses. Furthermore, Aloraini et al. [11] investigated how BaO impacts the protective capabilities of glasses, finding the maximum LAC at a BaO content of 20 mol%, and the values ranging between 0.0395 and 0.411 MeV, while at 0.0395 MeV the $Z_{eff}$ for the glasses with 10 mol% BaO was measured as 36.66. They concluded that increasing the BaO content further enhances the desirable radiation-protection characteristics of the glasses. Mhareb et al. [12] analyzed the impact of BaO doping on the physicochemical and shielding features of zinc sodium borate glasses, with the findings obtained via the Phy-X program revealing that the glass with the highest density (Ba-30) exhibited superior shielding performance. Sayyed et al. [13] reported that B2O3-ZnO-PbO-BaO glass compositions exhibited notable enhancements in both optical properties and radiation-shielding efficiency with the incorporation of BaO. Sriwongsa et al. [14] found changes in the optical and radiation-attenuation properties of the BaO-ZnO-Na2O-B2O3 glass with the reinforcement of BaO, demonstrating that replacing B2O3 with BaO enhanced the shielding capabilities against X- and gamma-rays. Effendy et al. [15] examined the mechanical and radiation-shielding properties of the BaO-Bi2O3-Al2O3-B2O3 glass system, indicating that the addition of BaO increased the MAC values, thus enhancing the shielding effectiveness of the synthesized glasses, with the glass containing 30 mol% BaO demonstrating the optimum performance among the produced samples. This study seeks to broaden the investigation of lead-free glass systems containing BaO through assessing their viability as transparent candidates for gamma-ray shielding materials. Glasses composed of B2O3-Na2O-Gd2O3 were synthesized with varying concentrations of BaO to develop effective radiation-shielding materials. The shielding capabilities of these glass materials were evaluated by assessing their MAC, HVL, and mean free path (MFP) values via the XCOM software, with their physical, mechanical, and optical features also examined in details.

## 2.Experimental aspects

### 2.1. Glass synthesis

The glass were synthesized with the formulation (70-x)B2O3-28Na2O-2Gd2O3-xBaO (where x = 0, 5, 10, 15, and 20 mol%) through the standard process of melt-quenching, and were labeled as B-00, B-05, B-10, B-15, and B-20, respectively, according to the amount of BaO introduced. All chemicals employed in the work, including H3BO3, Na2CO3, Gd2O3, and BaCO3, were of 99.9% purity and sourced from LOBA Chemie Pvt Ltd. The chemicals were weighed according to their stoichiometric ratios, and then combined and pulverized in an agate mortar to ensure a uniform blend. Next, the mixture was heated at 1050°C in a porcelain crucible for 1 h to yield a clear and bubble-free homogeneous molten glass solution, which was then poured onto a preheated brass plate and annealed at 300°C for two h to alleviate internal stresses and avoid cracking. Prior to characterization, the glasses were meticulously polished. **Fig. 1** presents a photograph of the developed glasses, while **Table 1** outlines the chemical composition and weight proportions of the elements for each type of glass.


**Fig. 1.** Picture of the fabricated glasses.

**Table 1.** Glass code, chemical composition, and weight fraction of the elements in each glass sample.

| Glass code | Chemical composition (mol%) | | | | Wt. fraction of the elements in each sample | | | | |
|---|---|---|---|---|---|---|---|---|---|
| | $B_2O_3$ | $Na_2O$ | $Gd_2O_3$ | BaO | B | O | Na | Gd | Ba |
| B-00 | 70 | 28 | 2 | 0 | 0.2174 | 0.5575 | 0.2077 | 0.0173 | 0.0000 |
| B-05 | 65 | 28 | 2 | 5 | 0.2018 | 0.5282 | 0.2077 | 0.0173 | 0.0448 |
| B-10 | 60 | 28 | 2 | 10 | 0.1863 | 0.4990 | 0.2077 | 0.0173 | 0.0896 |
| B-15 | 55 | 28 | 2 | 15 | 0.1708 | 0.4698 | 0.2077 | 0.0173 | 0.1343 |
| B-20 | 50 | 28 | 2 | 20 | 0.1553 | 0.4405 | 0.2077 | 0.0173 | 0.1792 |

## 2.2. Glass characterizations

### 2.2.1. X-ray diffraction and physical properties

The X-ray diffraction (XRD) patterns of the produced glasses were obtained through an X-ray diffractometer (Shimadzu XRD-7000 Maxima) configured with Bragg–Brentano geometry. The scans spanned a 2θ range from 10° to 80°, with a scanning rate of 2° per min and a step increment of 0.02°. The analysis utilized Cu-Kα radiation (λ = 1.5406 Å), with the diffractometer set to 30 mA and 40 kV. The densities of the glasses were assessed at ambient temperature using a digital scale (balance) (Shimadzu BL-220H) (precision: ±0.001 g). The Archimedes principle was applied, with toluene (density: $\rho_L$ = 0.867 g/cm³) employed as the immersion medium (liquid). The density was computed by utilizing the expression presented in Eq. 1 [12, 16]:

$$\rho = \frac{W_a}{W_a - W_L} \times \rho_L \quad (1)$$

where $W_a$ denotes the weight of the glass measured in air, $W_L$ refers to the weight when the glass is submerged in the liquid, and $\rho_L$ represents the density of the toluene. Through Eq. 2, the synthesized glasses' density (ρ) and molecular weight (M) were used to calculate the molar volume ($V_M$):

$$V_M = \frac{M}{\rho} \quad (2)$$

Meanwhile, Eqs. 3–6 determined the concentration of the ion ($N_{Ba}$), inter-ionic distance ($r_i$), polaron radius ($r_p$), and field strength ($F_S$), respectively [5, 17]:

$$N = \frac{mol\% \times \rho \times N_A}{M_W} \quad (3)$$

$$r_i = \left(\frac{1}{N}\right)^{1/3} \quad (4)$$

$$r_p = \left(\frac{1}{2}\right)\left(\frac{\pi}{6N}\right)^{1/3} \quad (5)$$

$$F_s = \frac{Z}{r_p^2} \quad (6)$$

where $N_A$ is Avogadro's number, M denotes the mean molecular weight, mol% indicates the barium (Ba) proportion, and Z is the atomic number of barium. The average separation between the boron atoms, $< d_{B-B} >$, was determined via the following relation:

$$< d_{B-B} > = \left(\frac{V_M^B}{N_A}\right)^{1/3} \quad (7)$$

$$V_M^B = \frac{V_M}{2(1-X_B)} \quad (8)$$

where $V_M^B$ describes the contained volume in 1 mole of boron in the glass matrix. Eqs. 9 and 10 were utilized to compute the oxygen molar volume ($V_o$) and oxygen packing density (OPD) of the glasses, respectively:

$$V_o = \frac{V_M}{n} \quad (9)$$

$$OPD = 1000 \times K \times \frac{\rho}{M_W} \quad (10)$$

where K is the number of oxygen atoms available in the glass composition.

### 2.2.2. Mechanical and UV-visible absorption studies

To gain a thorough perception of the practical applications of the prepared glasses, it is pivotal to assess their mechanical features. To achieve this, the Makishima and Mackenzie theoretical procedure was utilized to determine the glasses' elastic moduli, including the Young's modulus (Y), bulk modulus (B), shear modulus (S), and longitudinal modulus (L). Additionally, the Poisson's ratio (σ) and micro-hardness parameter (H) were computed. Y was defined as follows [5, 17]:

$$Y = 2G_tV_t \quad (11)$$

where Gt represents the dissociation density of the oxides present in the glass system, while $V_t$ indicates those oxides' packing density. If $x_i$ refers to the molar ratio of the $i^{th}$ element in the multi-oxides glass and $G_i$ indicates the dissociation energy of the oxides, the dissociation energy per unit volume ($G_t$) can be computed via Eq. 12:

$$G_t = \sum G_i x_i \quad (12)$$

The packing density factor ($V_t$) was evaluated through Eq. 13:

$$V_t = V_M \sum V_i x_i \quad (13)$$

where $V_i$ is the oxides' volume unit. The values of B, S, L, σ, and H were ascertained by utilizing Eqs. 14–18:

$$B = 1.2 V_t Y \quad (14)$$

$$S = \frac{3YB}{9B - Y} \quad (15)$$

$$L = B + \frac{4}{3} S \quad (16)$$

$$\sigma = \frac{Y}{2S} - 1 \quad (17)$$

$$H = \frac{(1 - 2\sigma)Y}{6(1 + \sigma)} \quad (18)$$

The UV-visible absorbance spectra of the glass samples were recorded with a UV-visible spectrophotometer (SHIMADZU, UV-2600) over the 200–1000 nm wavelength range (accuracy: ±0.1 nm) at room temperature. The coefficient of optical absorption α(ν) for a glass thickness t is described by Eq. 19 [5]:

$$\alpha(\nu) = \frac{2.303\, A(\lambda)}{t} \quad (19)$$

The indirect energy band gap ($E_g$) of the glasses was evaluated using Tauc's formula, expressed as follows:

$$(\alpha h\nu) = C(h\nu - E_g)^2 \quad (20)$$

where C is a constant, and hν describes the incident energy of the photon.

The Urbach energy ($E_U$) reflects the degree of disorder or randomness in the structural arrangement of the glass, and is calculated using Eq. 21 [17]:

$$\alpha = \alpha_0 \exp\left(\frac{h\nu}{E_U}\right) \quad (21)$$

where the constant $\alpha_0$ is referred to as the tailing parameter. Another optical parameter, the refractive index (n), was computed through Eq. 22:

$$\frac{(n^2 - 1)}{(n^2 + 2)} = 1 - \sqrt{\frac{E_g}{20}} \quad (22)$$

Other parameters, such as the dielectric constant (ε), reflection loss ($R_L$), molar refractivity ($R_M$), optical transmission (T), and metallization (M), were evaluated by utilizing the formulae provided in our earlier study [17].

### 2.2.3. Radiation-shielding properties

The MAC values were assessed using the XCOM software [18], applying the rule of mixtures as described by Eq. 23 [19]:

$$MAC = \sum_i w_i (MAC)_i \quad (23)$$

where $w_i$ denotes the weight % of the $i^{th}$ individual element. The glass thickness needed to reduce the intensity of the incident ray by 50% is known as the HVL, while the MFP is the distance over which the intensity of the incident ray falls to 1/e of its original value, calculated through Eqs. 24 and 25, respectively [17, 19]:

$$HVL = \frac{\ln 2}{\mu} \quad (24)$$

$$MFP = \frac{1}{\mu} \quad (25)$$

where μ is the LAC measured in $cm^{-1}$.

## 3. Results and discussion

### 3.1. X-ray diffraction analysis

The XRD patterns of the B-00 and B-20 glasses, as shown in **Fig. 2**, exhibit a single broad peak centered at 2θ = 29°. The lack of pronounced peaks in the spectra suggests that the samples have a non-crystalline nature, lacking long-range order. This examination supports the classification of the developed samples as glasses, since they do not display the char acteristic crystalline diffraction patterns expected of materials with ordered structures.

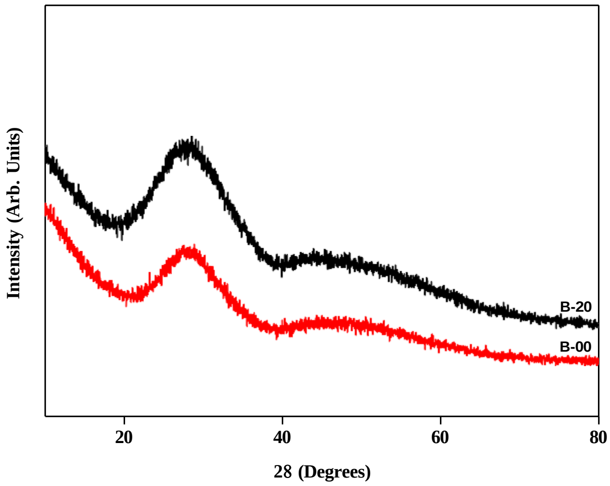


**Fig. 2.** XRD patterns of the B-00 and B-20 glass samples.

### 3.2. Physical parameters

**Table 2** presents the physical properties of the B-00–B-20 glasses, determined using expressions (1–10). The insertion of BaO results in an elevation of the density (ρ), barium ion concentration ($N_{Ba}$), molar volume of oxygen ($V_o$), and field strength ($F_s$) in the glasses. Conversely, the molar volume ($V_M$), distance between inter-ions ($r_i$), average boron–boron distance (< $d_{B-B}$ >), and OPD all decrease with increasing BaO content.

**Table 2.** Physical properties of the fabricated glasses.

| Property | Glass sample | | | | |
|---|---|---|---|---|---|
| | B-00 | B-05 | B-10 | B-15 | B-20 |
| Molecular weight, M (g/mol) | 70.409 | 74.595 | 78.780 | 82.965 | 87.158 |
| Density, ρ (g/cm$^3$) | 2.412 | 2.619 | 2.805 | 2.958 | 3.114 |
| Molar volume, $V_M$ (cm$^3$/mol) | 29.131 | 28.482 | 28.086 | 28.047 | 27.989 |
| Ion concentration, $N_{Ba}$ ($10^{23}$ ions/cm$^3$) | 0 | 1.057 | 2.144 | 3.221 | 4.303 |
| Polaron radius, $r_p$ ($10^{-8}$ m) | 0 | 2.814 | 2.223 | 1.941 | 1.763 |
| Inter-ionic distance, $r_i$ ($10^{-8}$ m) | 0 | 2.115 | 1.671 | 1.459 | 1.325 |
| Field strength, $F_s$ ($10^{17}$ cm$^{-2}$) | 0 | 0.808 | 1.295 | 1.698 | 2.060 |
| Average boron–boron separation, $< d_{B-B} >$ ($10^{-8}$ m) | 4.372 | 4.113 | 3.910 | 3.755 | 3.620 |
| Oxygen molar volume, $V_o$ (cm$^3$/mol) | 0.119 | 0.122 | 0.125 | 0.131 | 0.137 |
| Oxygen packing density, OPD (cm$^{-3}$ mol$^{-1}$) | 83.587 | 82.156 | 79.756 | 76.299 | 72.886 |

**Fig 3** shows the relationship between BaO loading and ρ and $V_M$. The increase in ρ can be ascribed to the replacement of the low molecular weight of $B_2O_3$ (69.6108 g/mol) with that of BaO (153.33 g/mol) [3, 10]. In contrast, the decline in $V_M$ with rising BaO content suggests a strengthening of the glass's compactness, also referred to as network shrinking. This phenomenon is characteristic of borate glasses, which are composed of a 3-D network of boron atoms bonded covalently to oxygen atoms [12, 20]. The loading of BaO to the glass network causes a substitution of B (boron) ions with $Ba^{2+}$ ions, resulting in a weakening of the borate matrix's linkage. This is obvious from the decreased $< d_{B-B} >$ and $V_M$ of the glasses. Consequently, the incorporation of BaO leads to glass samples that are structurally less dense and more pliable. Additionally, the extra presence of $Ba^{2+}$ ions in the glass host reduces $r_p$ and $r_i$, resulting in an increase in the $F_s$ values and thus indicating a strengthened relationship between the boron and $Ba^{2+}$ ions [21, 22, 23].

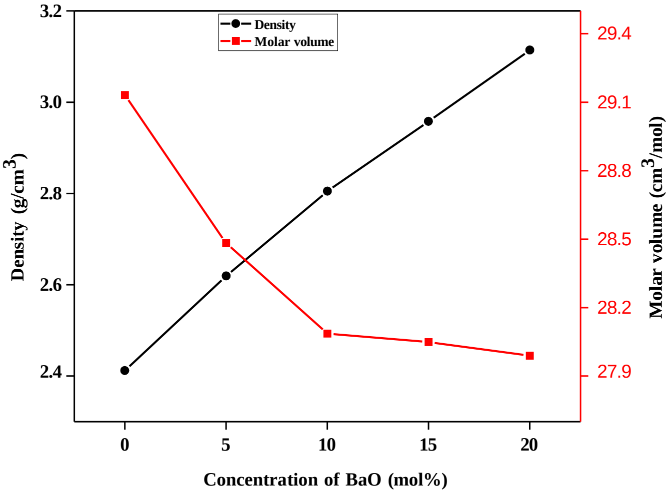


**Fig. 3.** Variation of the prepared glasses' density and molar volume with BaO concentration.

The replacement of B with Ba2+ in the glass host results in the formation of a considerable number of non-bridging oxygens (NBOs), which is associated with a reduction in the Eg values. This substitution also causes alterations in the Vo and OPD data [10, 24]. The study reveals an affirmative association between the levels of BaO incorporated into the glass matrix and Vo, reflecting an increase from 0.119 to 0.137 cm3/mol. Meanwhile, the OPD declines from 83.587 to 72.886, which signifies a widening of $V_o$ within the glass network since more space is occupied by oxygen atoms. Moreover, the noted drop in OPD is associated with a decline in density of the oxygen atoms.
The changes in OPD and $V_o$ relative to BaO concentration are illustrated in **Fig. 4**.

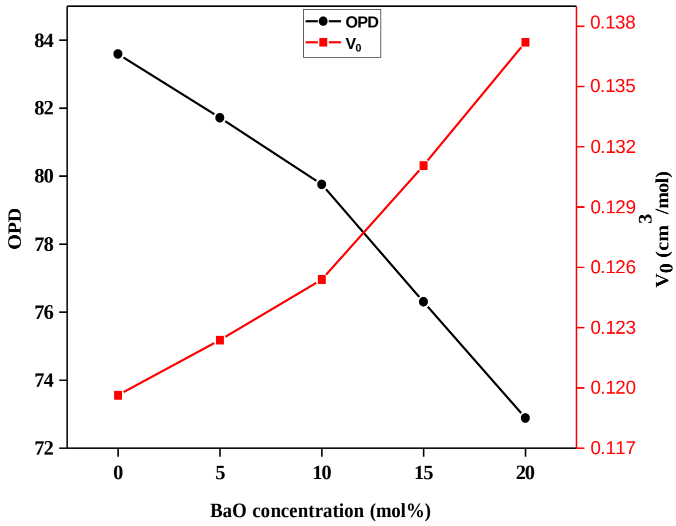


**Fig. 4.** Variation of the prepared glasses' OPD and $V_0$ with BaO concentration.

### 3.3. Mechanical studies

**Table 3** shows the theoretical values for $G_t$, $V_t$, and the elastic moduli for each composition of glass. As BaO is incorporated into the B-00–B-20 glasses, a small reduction in $V_t$ is observed, from 0.632 cm$^{-3}$ in the B-00 glass to 0.608 cm$^{-3}$ in the B-20 glass. This reduction is associated with the less ionic radius of $B_2O_3$ as compared to BaO. Additionally, $G_t$ declines from 68.408 kJ/m$^3$ in the B-00 glass to 59.748 kJ/m$^3$ in the B-20 glass as BaO replaces $B_2O_3$, which has a higher $G_i$ of 82.8 kJ/m$^3$ compared to BaO's $G_i$ of 40.6 kJ/m$^3$. The elastic moduli of the glasses exhibit a gradual decrease as BaO is incorporated, replacing $B_2O_3$ [25, 26]. Specifically, there is a decrease in the Young's modulus (Y) from 86.525 to 72.413 GPa, in the bulk modulus (B) from 65.664 to 52.757 GPa, in the shear modulus (S) from 33.788 to 28.491 GPa, and in the longitudinal modulus (L) from 110.715 to 90.645 GPa.

**Table 3.** Various mechanical properties for the prepared Ba series glasses.

| Glass sample | $V_t$ (cm$^{-3}$) | $G_t$ (KJ/cm$^3$) | Y (GPa) | B (GPa) | S (GPa) | L (GPa) | σ | H (GPa) |
|---|---|---|---|---|---|---|---|---|
| B-00 | 0.632 | 68.408 | 86.525 | 65.664 | 33.788 | 110.715 | 0.281 | 4.947 |
| B-05 | 0.631 | 66.243 | 84.127 | 64.104 | 32.829 | 107.877 | 0.280 | 4.787 |
| B-10 | 0.620 | 64.078 | 80.816 | 61.156 | 31.575 | 103.256 | 0.279 | 4.636 |
| B-15 | 0.618 | 61.913 | 76.535 | 56.767 | 30.008 | 96.776 | 0.275 | 4.495 |
| B-20 | 0.608 | 59.748 | 72.413 | 52.757 | 28.491 | 90.645 | 0.273 | 4.353 |

The variation of these mechanical moduli with increased BaO loading is depicted in **Fig. 5.** Furthermore, the hardness parameter decreases from 4.947 to 4.353 GPa as BaO is added, signaling a more expansive network structure within the glass. This structural change results in a weakening of the glass's overall integrity, leading to a reduction in elasticity and rigidity. The observed changes in mechanical properties are primarily attributed to the elevation in defects and voids, along with the creation of a substantial number of NBOs [26]. Notably, the Poisson's ratio is relatively unaffected by the addition of BaO, decreasing only slightly from 0.281 to 0.273 for the B-00 to B-20 samples, respectively. Of all the samples developed in this work, the B-00 sample demonstrates the optimum mechanical features.

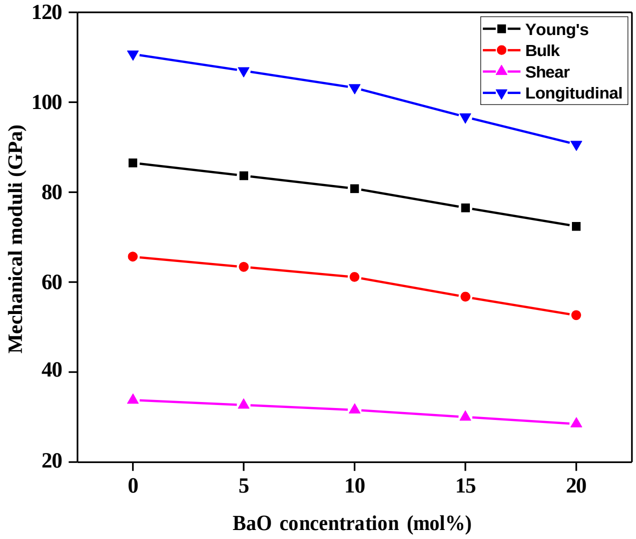


**Fig. 5.** Variation of the prepared glasses' mechanical moduli with BaO content.

### 3.4. Optical analysis

The UV-visible absorption spectra for the B-00–B-20 glasses are displayed in **Fig. 6.** The spectra reveal that the synthesized samples exhibit the absence of a sharp edge of absorption, indicating that they are glassy in nature. Upon examining the spectra, a prominent shift of the absorption edge toward higher wavelengths is observed as BaO is progressively introduced. The corresponding cut-off wavelengths can be deduced from these observations.

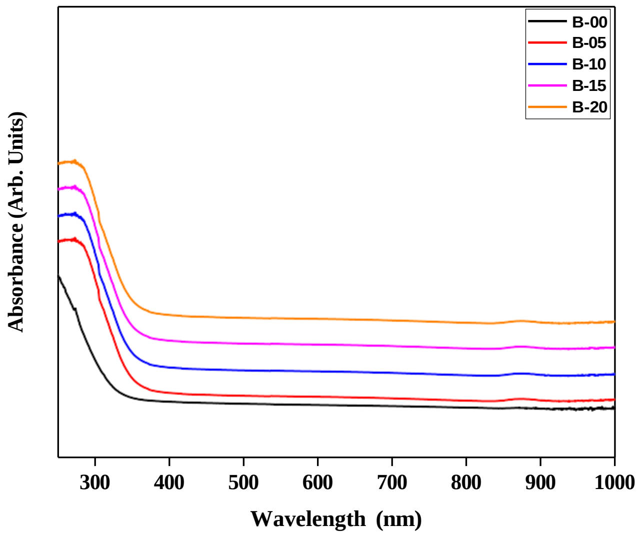


**Fig. 6.** Absorption spectra of the synthesized glass samples.

The optical characteristics of the current glasses were determined based on the UV absorption edge.**Table 4** presents all the computed optical properties for the fabricated glasses in this work. The optical bandgap ($E_g$) is a crucial parameter in optical studies, which can be utilized to calculate other parameters. $E_g$ is obtained using Eq. 20 by graphing $(\alpha h\nu)^{1/2}$ against hν, and extrapolating the linear segment to the point where $(\alpha h\nu)^{1/2} = 0$ for indirect transitions, as illustrated in **Fig. 7.** The $E_g$ values for the prepared glasses fall with increasing BaO content. This observation can be associated with the inclusion of $Ba^{2+}$ ions into the glass structure. The Ba ions differ significantly in size and charge from the ions of boron and oxygen in $B_2O_3$, leading to disruptions in the local network and the distribution of charges in the network. This results in the formation of defects such as NBO sites or vacancies of oxygens. Especially, the Ba ions function as electron donors, resulting in a higher concentration of donor centers in the structure with the addition of BaO. This elevated donor density in the glass structure results in a rise in the energy states of the donor oxygen ions, ultimately reducing the $E_g$ values [27, 28]. The Urbach energies ($E_U$) for all the examined glasses were calculated by determining the reciprocals of the slopes of the linear part in the lower photon energy range of the lnα versus hν plot, as displayed in **Fig. 8**. The calculated $E_U$ values are presented in **Table 4.** An increase in $E_U$ values with higher BaO content indicates a potential for local long-range order, likely due to an increase in the number of defects.The refractive index (n) of glass is a key parameter for identifying structural changes caused by variations in the composition of the glass system. In this study, we observed that replacing $B_2O_3$ with the high atomic mass, high field strength BaO results in an increase in n values from 2.384 to 2.449 (see **Table 4**). This effect is also ascribed to the increased atomic mass and enhanced polarizing capability of $Ba^{2+}$ ions relative to $B^{3+}$ ions [21, 29].

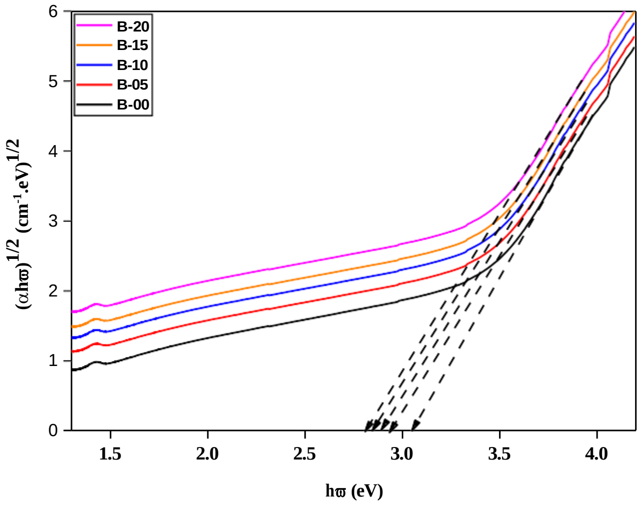


**Fig. 7.** Variation of the prepared glass samples' $(\alpha h\nu)^{1/2}$ with hν.

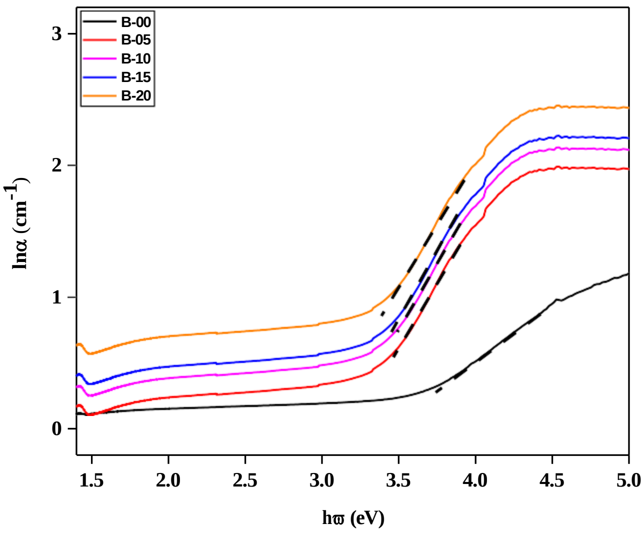


**Fig. 8.** Variation of the prepared glass samples' lnα with hν.

**Table 4.** Optical properties of the synthesized Ba-series glasses.

| Property | Glass sample | | | | |
|---|---|---|---|---|---|
| | **B-00** | **B-05** | **B-10** | **B-15** | **B-20** |
| Cut-off wavelength (nm) | 358 | 382 | 395 | 406 | 426 |
| Energy band gap, $E_g$ (eV) | 3.048 | 2.942 | 2.899 | 2.848 | 2.807 |
| Urbach energy, $E_U$ (eV) | 0.412 | 0.428 | 0.467 | 0.475 | 0.497 |
| Refractive index, n | 2.384 | 2.413 | 2.424 | 2.440 | 2.449 |
| Dielectric constant, ε | 5.683 | 5.823 | 5.876 | 5.954 | 5.998 |
| Molar refraction, $R_M$ ($cm^3$/mol) | 17.793 | 17.559 | 17.490 | 17.468 | 17.397 |
| Reflection loss, $R_L$ (%) | 16.727 | 17.140 | 17.296 | 17.523 | 17.650 |
| Metallization criteria, M | 0.390 | 0.384 | 0.381 | 0.377 | 0.375 |
| Optical transmission, T | 0.713 | 0.707 | 0.705 | 0.701 | 0.699 |

The dielectric constant (ε) increases as the n values rise, reflecting a greater number of NBOs. Consequently, $R_M$ declines and $R_L$ rises with increasing BaO content due to the increase in n values. The metallization (M) data for the produced glasses show a 0.390 to 0.375 reduction with changes in the BaO content. Importantly, these data consistently remained below 1, denoting a broadening of both the conduction and valence bands. Therefore, the non-conducting nature of the produced glasses decreases as the BaO concentration increases [30]. The variation of ε and M with BaO loading is depicted in **Fig. 9.** Furthermore, the optical transmission (T) values reduce as the concentration of BaO augments in the glasses [23].

### 3.5. Radiation-shielding features

We utilized the XCOM software [18] to evaluate the MAC of the glasses [18], with **Fig. 10** depicting the values over a wide energy spectrum from 0.015 to 15 MeV, which suggest that elevated BaO content is linked to increased MAC values. Notably, the MAC values show a consistent decrease as the photon energy rises, following an exponential decay pattern in line with the exponential law. This exponential reduction can be ascribed to three main processes of interaction: photoelectric absorption, Compton scattering, and pair production. At low energies, photoelectric absorption prevails, with a cross-section that fluctuates with energy as $E^{-3.5}$ and the atomic number as $Z^4$. This process is especially significant near the Ba's K-shell edge of absorption, where the energy of the K-shell is approximately 38.44 keV, leading to a tip in the MAC around 0.04 MeV. As the photon energies increase from 400 keV to 1 MeV, Compton scattering becomes the dominant process, with the cross-section dependent on energy as $E^{-1}$ and for the atomic number as Z. Above the energy threshold of 1.05 MeV, pair production becomes the foremost interaction process. These findings are consistent with the results reported in references [31–34].

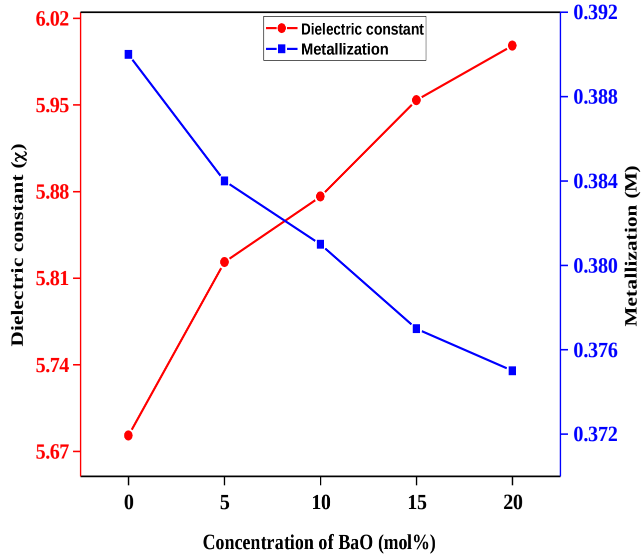


**Fig. 9.** Variation of ε and M with BaO concentration.

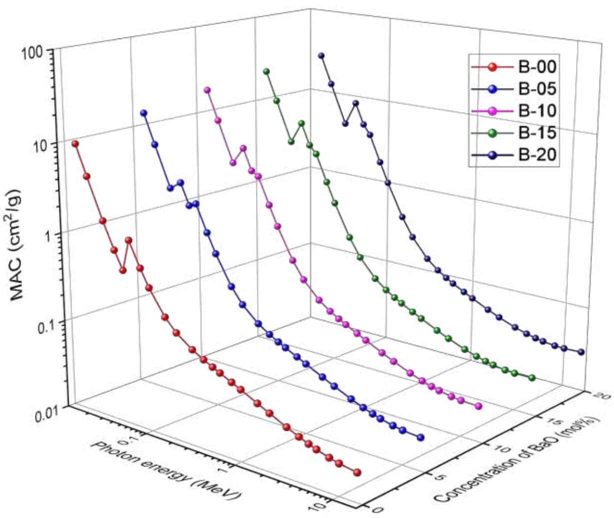


**Fig. 10.** Variation of the prepared glasses' MAC with photon energy and BaO concentration.

**Fig. 11 (a–c)** illustrates how the MAC values vary with BaO concentration across different energy ranges (low, medium, and high) from 0.015 to 15 MeV, where the BaO loadings have a noticeable effect on the MAC values. This parameter reveals an upward trend for lower, medium, and higher energies with additional BaO concentrations ranging from 0 to 20 mol%, where these patterns can be attributed to the impact of BaO on the structural changes in the manufactured glasses, including their elevated density from 2.412 to 3.114 g/cm$^3$. It is widely accepted that density is a crucial factor in boosting a medium's ability to reduce radiation photons. Moreover, MAC values are affected not only by photon energies but also by the mass density of the shield or barrier, since the photon energy affects how changes in the MAC values correlate with the density [34, 35]. To utilize Ba-doped glasses for radiation protection, it is important to compare the B-20 glass sample (featuring elevated BaO content) against other established shielding concretes, such as standard, barite, and hematite, and commercial window glasses such as RS-360 and RS-253, as well as various other BaO-doped glasses. This comparison is displayed in **Fig. 12** and detailed in **Table 5**, which lists the MAC values at 0.662 MeV. From the figure, we observe that the MAC value of the B-20 glass is marginally higher than those of the other shielding glasses and concretes, excluding RS-360. Thus, we can affirm that our glass samples (and particularly B-20) exhibit excellent protective capability in the context of radiation shielding.

**Table 5.** Comparison of the MAC values for the B-20 glass with certain standard concretes, shielding glasses, and glasses containing BaO at 0.662 MeV.

| Glass sample | MAC (cm$^2$/g) | Reference(s) |
|---|---|---|
| B-20 | 0.0779 | **Present work** |
| Barite concrete | 0.0780 | **[37, 38]** |
| Ordinary concrete | 0.0778 | **[37, 38]** |
| Hematite serpentine | 0.0770 | **[37, 38]** |
| RS-360 | 0.0889 | **[21]** |
| RS-253 | 0.0754 | **[21]** |
| S3 | 0.0763 | **[23]** |
| G3 | 0.0765 | **[39]** |
| SBC-B20 | 0.0773 | **[40]** |

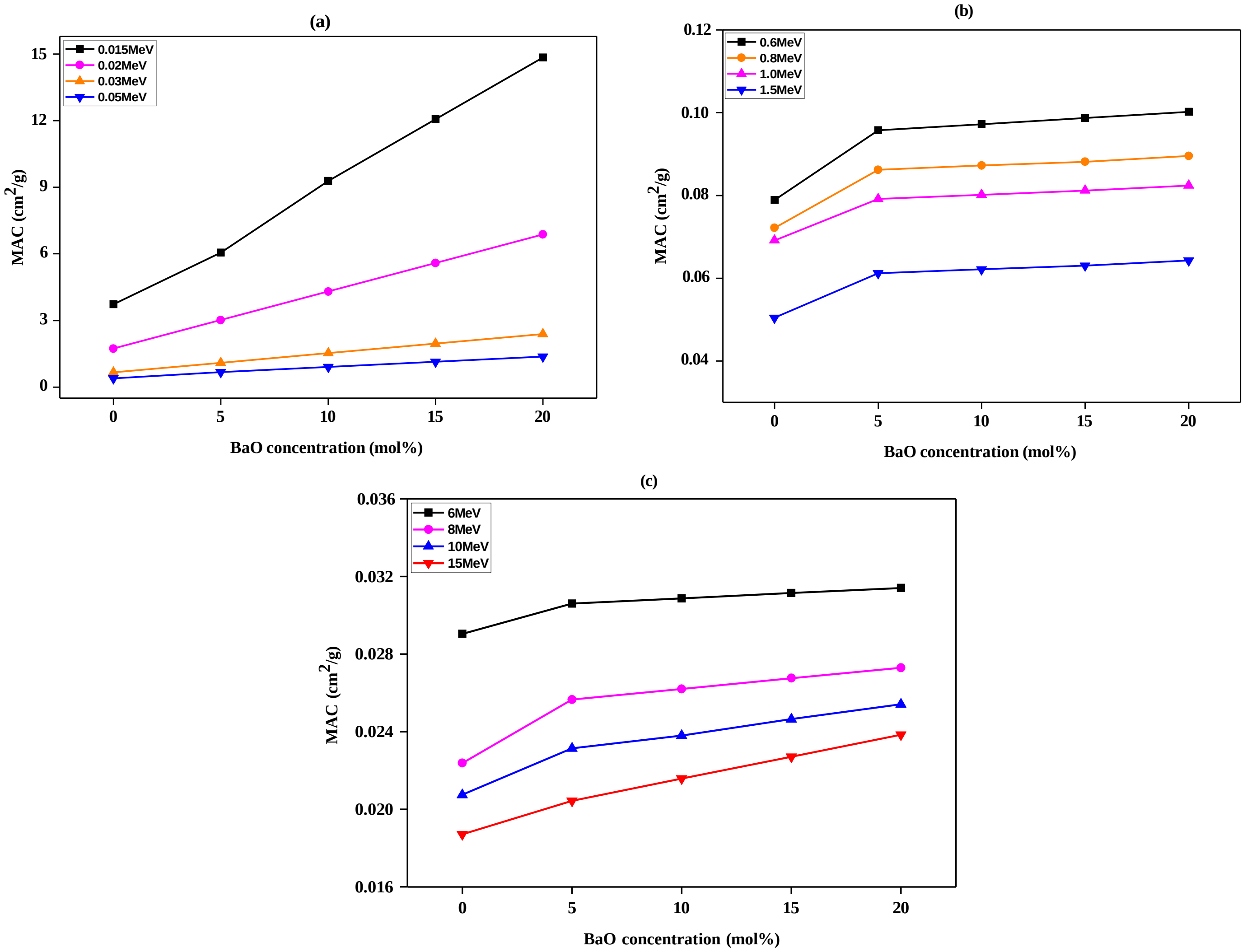


**Fig. 11.** Variation of the prepared glasses' MAC with BaO concentration at a) lower energies, b) mid-energies, and c) higher energies.

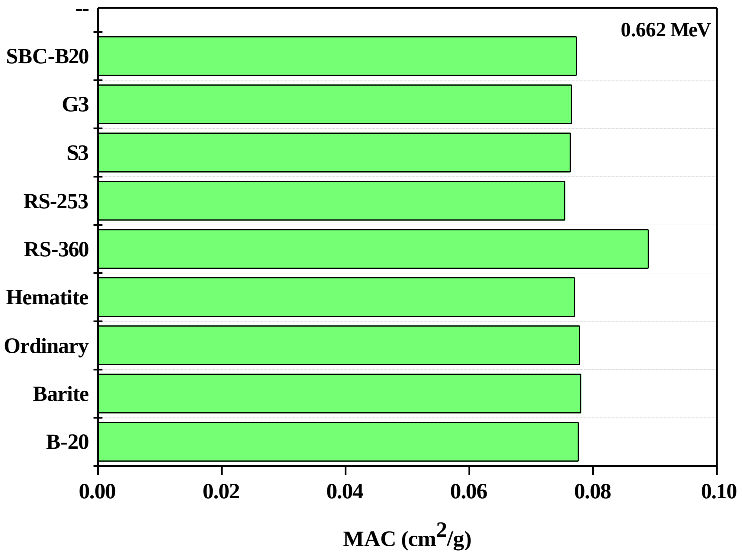


**Fig. 12.** Comparison of the MAC for the Ba-20 glass against standard materials and other glasses containing BaO at 0.662 MeV.

Furthermore, the HVL (evaluated through Eq. 24) is a key factor in assessing the capability of protecting materials. **Fig. 13** shows the variation in HVL with photon energy for different BaO concentrations. The HVL values start with low readings from 0.015 to 0.03 MeV, followed by a steep drop from 0.03 to 0.04 MeV, and then a rapid rise from 0.04 to 15 MeV. All the current glasses present similar patterns in HVL values with respect to the photon energies. This behavior can be explained as follows: at low energies, photoelectric interactions require thin glasses (resulting in low HVL values); secondary Compton scattering demands thicker glasses (leading to higher HVL values) at medium energies; and at high photon energy levels, significant photons can pass through the material. These findings are in agreement with the results documented in previous works [32, 34, 36]. Additionally, the MFP (evaluated via Eq. 25) is an important indicator for determining the radiation-shielding effectiveness of materials, with **Fig. 14** demonstrating how the MFP varies with photon energy for the produced glass. The lowest MFP values occur between 0.015 and 0.03 MeV, followed by a steep drop from 0.03 to 0.04 MeV, and then a rapid rise from 0.04 to 15 MeV. According to these observations, the greatest MFP is linked with the photon energy of 15 MeV. The material can attenuate a lower flux of high-energy photons and a greater flux of low-energy photons. Higher MFP values suggest that thicker glasses are more suitable for radiation-protection purposes. These findings are in agreement with the results documented in previous works [32, 34, 36].

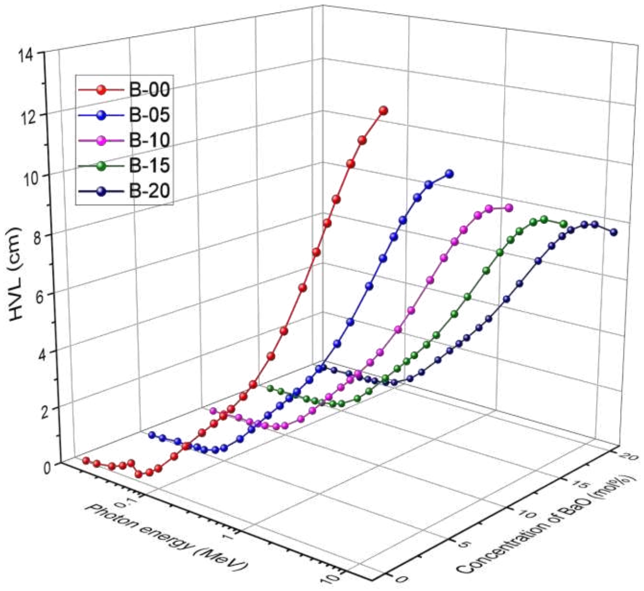


**Fig. 13.** Variation of the prepared glasses' HVL with photon energy and BaO concentration.

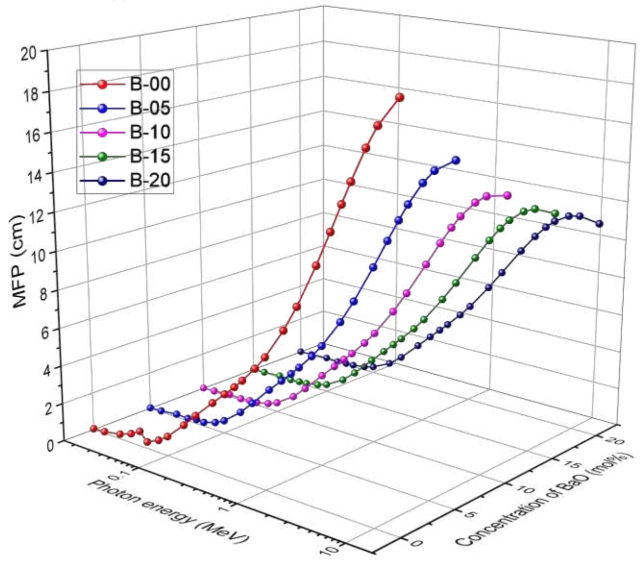


**Fig. 14.** Variation of the prepared glasses' MFP with photon energy and BaO concentration.

## Conclusion

This study provides an extensive understanding of the physical, mechanical, optical, and radiation-attenuation features of $B_2O_3$-$Na_2O$-$Gd_2O_3$ glasses doped with BaO. The glasses were prepared via the standard melt-quenching technique. XRD analysis revealed that the glasses were amorphous, as indicated by the lack of clear peaks in the patterns. The density of the glasses increased from 2.412 to 3.114 g/cm$^3$ with rising BaO concentration, while the mechanical moduli decreased, namely, the Young's modulus (Y) from 86.525 to 72.413 GPa, the bulk modulus (B) from 65.664 to 52.757 GPa, the shear modulus (S) from 33.788 to 28.491 GPa, and the longitudinal modulus (L) from 110.715 to 90.645 GPa, thus indicating a decline in the rigidity of the glasses. The reduction in optical band gap energy from 3.048 to 2.807 eV and elevation in refractive index from 2.384 to 2.449 suggests that the incorporation of BaO leads to an increase in NBO quantity. Additionally, the increase in Urbach energy from 0.412 to 0.497 eV suggests the formation of more defects in the glasses. In terms of the radiation-shielding properties, the loading of BaO led to improved MAC values. The B-20 sample, which contains 20 mol% BaO, demonstrated the highest MAC (0.0779 cm$^2$/g at 0.662 MeV) and the smallest HVL and MFP values among the glass samples tested, thus rending it the most viable choice for gamma-ray shielding applications. Furthermore, the comparison of the evaluated MAC values with established shielding materials and other BaO-doped glasses confirmed that the glass with the highest BaO concentration (20 mol%) offers superior radiation-attenuation effectiveness and is therefore well-suited for protection applications, particularly at lower energies. In conclusion, our glasses provide valuable insights for future research and practical applications.

## References

[1] A. Samir, M.A. Hassan, F. Ahmad, M.S. Sadeq, S.Y. Marzouk, H.Y. Morshidy, Impacts of BaO additives on the mechanical, optical and radiation shielding properties of BaO–K2O–CoO–Al2O3–B2O3 glasses, Optical Materials, 143 (2023) 114195.

[2] Manjunatha, A.S. Bennal, M.M. Hosamani, G.B. Hiremath, V.P. Singh, N.M. Badiger, Experimental investigation of gamma-ray interaction parameters and buildup factors in lanthanide compounds: Insights into penetration depth, Applied Radiation and Isotopes, 212 (2024) 111466.

[3] H.M.H. Zakaly, H.A. Saudi, S.A.M. Issa, M. Rashad, A.I. Elazaka, H.O. Tekin, Y.B. Saddeek, Alteration of optical, structural, mechanical durability and nuclear radiation attenuation properties of barium borosilicate glasses through BaO reinforcement: Experimental and numerical analyses, Ceramics International, 47 (2021) 5587–5596.

[4] M.I. Sayyed, H.Y. Morshidy, K.S. Shaaban, A.F.A. El-Rehim, A.M. Ali, M.S. Sadeq, Impacts of BaO additions on structure, linear/nonlinear optical properties and radiation shielding competence of BaO–NiO–ZnO–B2O3 glasses, Optical Materials, 144 (2023) 114300.

[5] S. Biradar, M.N. Chandrashekara, Manjunatha, A. Dinkar, G.B. Devidas, A.S. Bennal, R. Rajaramakrishna, M.I. Sayyed, Synergistic optimization of physical, thermal, structural, mechanical, optical and radiation shielding characteristics in borate glasses doped with Bi2O3, Optical Materials, (2024) 115815.

[6] A.M.A. Mostafa, S.A.M. Issa, E.F. El Agammy, H.M.H. Zakaly, B.M. Alotaibi, F. Gharghar, Effect of BaO addition on gamma radiation shielding performance of sodium barium borate glasses using FLUKA code and PhyX/PSD platform, Radiation Physics and Chemistry, 206 (2023) 110766.

[7] M.I. Sayyed, M.H.A. Mhareb, Y.S.M. Alajerami, K.A. Mahmoud, M.A. Imheidat, F. Alshahri, M. Alqahtani, T. Al-Abdullah, Optical and radiation shielding features for a new series of borate glass samples, Optik, 239 (2021) 166790.

[8] P. Limkitjaroenporn, J. Kaewkhao, P. Limsuwan, W. Chewpraditkul, Physical, optical, structural and gamma-ray shielding properties of lead sodium borate glasses, Journal of Physics and Chemistry of Solids, 72 (2011) 245–251.

[9] Y. Al-Hadeethi, M.I. Sayyed, J. Kaewkhao, B.M. Raffah, R. Almalki, R. Rajaramakrishna, An extensive investigation of physical, optical and radiation shielding properties for borate

glasses modified with gadolinium oxide, Applied Physics A, 125 (2019) 1–10.

[10] S. Biradar, A. Dinkar, Manjunatha, A.S. Bennal, G.B. Devidas, B.T. Hareesh, M.K. Siri, K.N. Nandan, M.I. Sayyed, H. Es-soufi, M.N. Chandrashekara, Comprehensive investigation of borate-based glasses doped with BaO: An assessment of physical, structural, thermal, optical, and radiation shielding properties, Optical Materials, 150 (2024) 115176.

[11] D.A. Aloraini, A. Kumar, A.H. Almuqrin, M.I. Sayyed, Optical and gamma ray shielding properties BaO doped K2O-TiO2-P2O5 glasses, Optik (Stuttg), 247 (2021) 167893.

[12] M.H.A. Mhareb, M. Alqahtani, F. Alshahri, Y.S.M. Alajerami, N. Saleh, N. Alonizan, M.I. Sayyed, M.G.B. Ashiq, T. Ghrib, S.I. Al-Dhafar, The impact of barium oxide on physical, structural, optical, and shielding features of sodium zinc borate glass, Journal of Non-Crystalline Solids, 541 (2020) 120090.

[13] M.I. Sayyed, K.A. Mahmoud, K.M. Kaky, Exploring the BaO/B2O3 substitution impacts on B2O3-ZnO-PbO-BaO glasses: Comprehensive analysis for physical, optical, mechanical, and radiation shielding properties, Annals of Nuclear Energy, 208 (2024) 110765.

[14] K. Sriwongsa, S. Ravangvong, P. Glumglomchit, S. Kaewjaeng, N. Intachai, S. Kothan, C. Mutuwong, J. Kaewkhao, The investigation of physical, optical, X/gamma-rays and thermal neutron shielding properties using experimental, simulation, and theoretical for BaO-based glass system, Radiation Physics and Chemistry, 222 (2024) 111841.

[15] N. Effendy, M.H.M. Zaid, K.A. Matori, S.M. Iskandar, R. Hisam, M.N. Azlan, N.N. Yusof, H.M.H. Zakaly, S.A.M. Issa, Y.B. Saddeek, Fabrication of novel BaO–Al2O3–Bi2O3–B2O3 glass system: Comprehensive study on elastic, mechanical and shielding properties, Progress in Nuclear Energy, 153 (2022) 104418.

[16] D.G. Byalollikar, S. Biradar, A. Dinkar, T. Sankarappa, J. Biradar, Impact of bismuth oxide on structural, optical and gamma-ray shielding properties of calcium–sodium–borate glasses, Radiation Protection Dosimetry, 200 (2024) 1207–1215.

[17] S. Biradar, M.N. Chandrashekara, A. Dinkar, Manjunatha, G.B. Devidas, A.S. Bennal, M.I. Sayyed, H. Es-soufi, A multifaceted study of B2O3-BaO-PbO-WO3 glasses doped with Bi2O3: Insights from physical, thermal, structural, mechanical and optical analyses towards improved shielding properties, Ceramics International, 50 (2024) 29332–29345.

[18] M.G. Dong, M.I. Sayyed, G. Lakshminarayana, M. Çelikbilek Ersundu, A.E. Ersundu, P. Nayar, M.A. Mahdi, Investigation of gamma radiation shielding properties of lithium zinc bismuth borate glasses using XCOM program and MCNP5 code, Journal of Non-Crystalline Solids, 468 (2017) 12–16.

[19] Manjunatha, M.M. Hosamani, G.B. Hiremath, A. Vinayak, V.P. Singh, A.S. Bennal, N.M. Badiger, An experimental approach to determine the gamma radiation interaction mean free path and exposure buildup factor for biomolecules, Applied Radiation and Isotopes, (2023) 111012.

[20] B.O. El-Bashir, M.I. Sayyed, M.H.M. Zaid, K.A. Matori, Comprehensive study on physical, elastic and shielding properties of ternary BaO-Bi2O3-P2O5 glasses as a potent radiation shielding material, Journal of Non-Crystalline Solids, 468 (2017) 92–99.

[21] A. Aboalatta, J. Asad, M. Humaid, H. Musleh, S.K.K. Shaat, K. Ramadan, M.I. Sayyed, Y. Alajerami, N. Aldahoudi, Experimental investigation of zinc sodium borate glass systems containing barium oxide for gamma radiation shielding applications, Nuclear Engineering and Technology, 53 (2021) 3058–3067.

[22] M.H.A. Mhareb, Y.S.M. Alajerami, M.I. Sayyed, N. Dwaikat, M. Alqahtani, F. Alshahri, N. Saleh, N. Alonizan, T. Ghrib, S.I. Al-Dhafar, Radiation shielding, structural, physical, and optical properties for a series of borosilicate glass, Journal of Non-Crystalline Solids, 550 (2020) 120360.

[23] P. Kaur, K.J. Singh, M. Kurudirek, S. Thakur, Study of environment friendly bismuth incorporated lithium borate glass system for structural, gamma-ray and fast neutron shielding properties, Spectrochimica Acta Part A: Molecular and Biomolecular Spectroscopy, 223 (2019) 117309.

[24] H.A. Saudi, H.O. Tekin, H.M.H. Zakaly, S.A.M. Issa, G. Susoy, M. Zhukovsky, The impact of samarium (III) oxide on structural, optical and radiation shielding properties of thallium-borate glasses: Experimental and numerical investigation, Optical Materials, 114 (2021) 110948.

[25] M.I. Sayyed, K.A. Mahmoud, J. Arayro, Y. Maghrbi, M.H.A. Mhareb, An extensive assessment of the impacts of BaO on the mechanical and gamma-ray attenuation properties of lead borosilicate glass, Scientific Reports, 14 (2024) 5429.

[26] F.H.F. Al-Saeedi, M.I. Sayyed, F.L. Kapustin, H. Al-Ghamdi, E.V. Kolobkova, O.L. Tashlykov, A.H. Almuqrin, K.A. Mahmoud, A novel barium oxide-based Iraqi sand glass to attenuate the low gamma-ray energies: Fabrication, mechanical, and radiation protection capacity evaluation, Nuclear Engineering and Technology, 54 (2022) 3051–3058.

[27] A. Kumar, R. Kaur, M.I. Sayyed, M. Rashad, M. Singh, A.M. Ali, Physical, structural, optical and gamma ray shielding behavior of (20+x) PbO–10 BaO–10 Na2O–10 MgO–(50-x) B2O3 glasses, Physica B: Condensed Matter, 552 (2019) 110–118.

[28] S.H. Alazoumi, S.A. Aziz, R. El-Mallawany, U.S. Aliyu, H.M. Kamari, M.H.M.M. Zaid, K.A. Matori, A. Ushah, Optical properties of zinc lead tellurite glasses, Results in Physics, 9 (2018) 1371–1376.

[29] K.M. Kaky, M.I. Sayyed, M.K. Hamad, S. Biradar, M.H.A. Mhareb, U. Altimari, M.M. Taki, Bismuth oxide effects on optical, structural, mechanical, and radiation shielding features of borosilicate glasses, Optical Materials, 155 (2024) 115853.

[30] M.I. Sayyed, M.J. Zaiter, M.H.A. Mhareb, K.A. Mahmoud, S. Biradar, R.I. Mahdi, K.M. Kaky, Optical, physical, mechanical, structural, and radiation shielding investigations of B2O3–TeO2–GeO2–MgO–PbO for ionizing protection and optical transmission application, Optical Materials, 154 (2024) 115807.

[31] M.I. Sayyed, A. Saleh, A. Kumar, F.E. Mansour, Experimental examination on physical and radiation shielding features of borosilicate glasses doped with varying amounts of BaO, Nuclear Engineering and Technology, 56 (2024) 3378–3384.

[32] M.I. Sayyed, U. Rilwan, K.A. Mahmoud, M. Elsafi, Experimental study of the radiation shielding characteristics of new PbO–Na2O–B2O3–BaO glasses, Nuclear Engineering and Technology, (2024).

[33] A.S. Abouhaswa, H.O. Tekin, E.M. Ahmed, O. Kilicoglu, Y.S. Rammah, Synthesis, physical, linear optical and nuclear radiation shielding characteristics of B2O3–BaO–PbO–SrO2 glasses, Journal of Materials Science: Materials in Electronics, 32 (2021) 18163–18177.

[34] A. Saeed, Y.H. Elbashar, R.M. El Shazly, Optical properties of high density barium borate glass for gamma ray shielding applications, Optical and Quantum Electronics, 48 (2016) 1–10.
[35] K.M. Kaky, M.I. Sayyed, K.A. Mahmoud, M.H.A. Mhareb, S. Biradar, A.J. Kadhim, A comprehensive investigation on lanthanum ions doped borate-tellurite-germinate glass for radiation shielding and optical application, Progress in Nuclear Energy, 176 (2024) 105402.
[36] M.I. Sayyed, S.A.M. Issa, H.O. Tekin, Y.B. Saddeek, Comparative study of gamma-ray shielding and elastic properties of BaO–Bi2O3–B2O3 and ZnO–Bi2O3–B2O3 glass systems, Materials Chemistry and Physics, 217 (2018) 11–22.
[37] S. Sharifi, R. Bagheri, S.P. Shirmardi, Comparison of shielding properties for ordinary, barite, serpentine and steel–magnetite concretes using MCNP-4C code and available experimental results, Annals of Nuclear Energy, 53 (2013) 529–534.
[38] C. Bootjomchai, J. Laopaiboon, C. Yenchai, R. Laopaiboon, Gamma-ray shielding and structural properties of barium–bismuth–borosilicate glasses, Radiation Physics and Chemistry, 81 (2012) 785–790.
[39] M.H.A. Mhareb, M.I. Sayyed, Y.S.M. Alajerami, M. Alqahtani, N. Dwaikat, A.M. Alsagry, M. Al-Yatimi, M. Zakariah, Structural and radiation shielding features for a new series of borate glass samples: Part I, European Physical Journal Plus, 136 (2021) 1–15.
[40] M.S. Al-Buriahi, C. Sriwunkum, H. Arslan, B.T. Tonguc, M.A. Bourham, Investigation of barium borate glasses for radiation shielding applications, Applied Physics A, 126 (2020) 68.